Improved Fault Location through Analysis of System Parameters during Auto-Reclose Operations on Transmission Lines

Liang Ji, Campbell Booth, Adam Dyśko, Member, IEEE, Fumio Kawano, Member, IEEE, Phil Beaumont, Senior Member, IEEE

Abstract—This paper describes a novel single-ended impedance based fault location method for transmission lines, which is based upon analysis of voltage and current during discrete system states that arise during the operation of single and three phase auto-reclose schemes. A fault location estimation algorithm, using the data measured during various system states and is capable of locating the fault types involving one fault resistance (i.e. single line-to-ground fault or line-to-line fault), is developed and presented. The proposed fault location technique is shown to have a high accuracy; results are presented and compared with the well-established Takagi method and the performance of the algorithm is analyzed and discussed. The proposed technique can reduce or negate limitations associated with conventional single-ended methods and can also estimate other factors associated with the fault, e.g. fault resistance and remote source impedance. Additionally, it is a potentially economic solution, as it is relatively straightforward to implement on a standard protection relay hardware platform. The proposed method is demonstrated using EMTP/ATP simulation models for a variety of different cases. The paper concludes with an overview of ongoing and future work that has the intention of moving the work forward towards implementation within commercially available relay hardware.

Index Terms—auto-reclose scheme, single-ended fault location method

NOMENCLATURE

CB	Circuit Breaker
SPAR	Single Phase Auto Reclose Scheme
TPAR	Three Phase Auto Reclose Scheme
γ	Propagation constant of transmission line
d	Transmission line length
Z_c	Surge impedance of transmission line
n	Fault location as a proportion of total line length
R_f	Fault resistance
Z_f	Fault impedance
$\mathbf{K}$	Weighted fault type matrix
SCL1, SCL2	Local and remote end short circuit levels
$\mathbf{Z_{loc}}$,$\mathbf{Z_{rem}}$	Local and remote end impedances
$\mathbf{V_L}$, $\mathbf{I_L}$	Local end voltage and current during pre-fault state
$\mathbf{V_R}$, $\mathbf{I_R}$	Remote end voltage and current during pre-fault state
$\mathbf{E_f}$	Voltage at the fault location in the pre-fault network
$\mathbf{V_{1L}}$, $\mathbf{I_{1L}}$	Local end voltage and current during state 1
$\mathbf{V_{1R}}$, $\mathbf{I_{1R}}$	Remote end voltage and current during state 1
$\mathbf{V_{2L}}$, $\mathbf{I_{2L}}$	Local end voltage and current during state 2
Z_{rs}	Self impedance of remote end source
Z_{rm}	Mutual impedance of remote end source

Matrices are denoted by bold in the text above.

Manuscript received June 11, 2012. This work was supported by University of Strathclyde, UK and Toshiba International (Europe) Ltd.

Liang Ji is with the University of Strathclyde, UK. (Corresponding author; phone: 0044-141-548-2120; E-mail: liang.ji@strath.ac.uk).

Campbell Booth is with the University of Strathclyde, UK. (E-mail: c.booth@eee.strath.ac.uk).

Adam Dysko is with the University of Strathclyde, UK. (E-mail: a.dysko@strath.ac.uk).

Fumio Kawano is with Toshiba International (Europe) Limited, Durham, UK. (E-mail: kawanof@til.toshiba-global.com)

Phil Beaumont is with Toshiba International (Europe) Limited, Durham, UK. (E-mail : philb@til.toshiba-global.com)

Shogo Miura is with Toshiba Corporation, Tokyo, Japan. (E-mail: shogo2.miura@toshiba.co.jp)

I. INTRODUCTION

Fast and accurate fault location processes are essential to reduce the duration of outages, facilitate remedial and maintenance work and hence improve system availability [1].

Impedance based fault location methods are widely utilized in modern power networks. The accuracy of typical single ended impedance method [2]-[3]can be affected by differences in fault resistance, uncertainty over assumed remote source impedance and pre-fault load flow. The techniques introduced in [4] and [5] have improved fault location capabilities by requiring remote end information (e.g. remote end infeed); mainly through reducing the effects of variations in fault resistance on location accuracy. In [7]-[10], fault location techniques using data from both ends of the faulted feeder have been introduced. Ensuring that the measurement data from each end of the line are in synchronism is a critical factor that influences location accuracy in such two-ended schemes. GPS time coding techniques [9]-[10] have been utilized in two-ended applications in order to improve the synchronism of the measurement data at each end of the line.

[11] and [12] introduce travelling wave based fault location techniques. Such techniques can greatly increase fault location accuracy. However, there are difficulties with such methods, e.g. problems associated with wavefront detection, timing accuracy, processing multiple reflections and issues with filtering of noise [1].

The fault location algorithm presented in [17] incorporates analysis of data during CB operations. During a three-phase CB

operation, each of the three poles does not open simultaneously. The individual current zero crossings for each phase, which are the points around which current interruption usually occurs, are displaced by 120° (corresponding to several milliseconds in 50/60Hz systems). Accordingly, several discrete states, which are defined as interpole states, arise due to the progression of the three-phase circuit breaking phenomenon. The fault location method outlined in this paper is based on modeling of interpole states and can achieve very accurate fault location only using single ended data. However, the interval between interpole states is typically 3.3ms for a 50Hz system (this may vary under certain conditions) [17]. It is difficult to extract fundamental frequency phasors in such a short time window and the accuracy of the algorithm may be compromised.

Therefore, the method has been extended to also analyze auto-reclose data in addition to the original fault data. This will, for permanent faults, allow the algorithm to have more time and data to establish an accurate fault location. Both SPAR and TPAR schemes are analyzed; these are widely implemented by power utilities [13]-[14]. Only permanent faults are analyzed; these obviously represent the class of faults that are of most interest to the operators, in terms of accurate location to facilitate timely repair.

The analysis of voltage and current data during different states of the auto-reclose scheme is fundamental to this technique. System data is divided into appropriate intervals representing the discrete states and subsequently processed to obtain individual current and voltage phasors during each state. The fault location estimation system, based on the modeling of behavior during the various states, is then executed. In this paper, permanent single line to ground faults form the focus of investigation – of permanent faults, these are the most common category. A transmission line model with source infeeds at each end (during the fault) is used as the basis for implementation and investigation.

II. AUTO-RECLOSE SCHEMES

A. Introduction

Faults on transmission lines are either transient or permanent. Auto-reclosing schemes are often incorporated to open and reclose the CB(s) after initial fault clearance so that supply may be quickly restored in the event of a transient (e.g. due to lightning) fault. In the case of a permanent fault (e.g. due to irrecoverable failure of insulation) the CB will reclose on to the fault, the protection will re-trip and subsequently "lockout" (sometimes after multiple re-close attempts), after which the fault will require to be repaired before return to service [13].

In SPAR schemes, only the faulted phase is tripped. In a transmission line with infeed sources at both ends, which is the typical arrangement in an interconnected power system, the poles corresponding to the faulted phase of the CBs at each end of the circuit should theoretically open and reclose simultaneously for both transient and permanent faults. However, the measurement devices, protection relays and CBs will suffer stress on two occasions for permanent faults with SPAR schemes. With the help of communication channels and differential protection, [15] proposed a modified SPAR scheme, which initially recloses only a single CB at one end of the line. If this operation results in a "close on to fault" situation, the reclosed CB will be re-tripped by the protection and the other end breaker(s) will remain open. For transient faults, the other end CB(s) will be reclosed after receiving data that indicates the fault is transient.

This modified SPAR scheme and practical experience in SPAR operation means that there is typically an interval between the reclosing of the individual CBs in SPAR schemes. This interval can be assumed to be of sufficient duration to enable the fundamental frequency component to be extracted from the measurement data.

In TPAR schemes, all three phases are tripped, regardless of the type of fault. In the case of a transient fault, after initial clearance and a predetermined delay, one CB will reclose and then the other end(s) will reclose after a synchronism check. In the case of a permanent fault, the initially reclosed CB will be re-tripped to clear the fault and the other CB will remain open.

Fig. 1 illustrates the currents measured at one end of the circuit (termed the "local end"), during simulated operation of a SPAR scheme Fig. 1 (a) presents the local currents where the local CB is reclosed first after initial fault clearance, while Fig. 1(b) illustrates the same situation, but with the remote CB being reclosed first. Refer to Section III of this paper for a more detailed description of the model used in simulations.

The waveforms associated with a TPAR scheme are similar a SPAR scheme, with three phases opening and reclosing.

In both SPAR and TPAR schemes, there are effectively five individual system states (as seen in Fig. 1) for a permanent fault scenario:

- State A: Pre-fault state, both line end CBs closed.
- State B: During-fault state, both CBs remain closed.
- State C: Initial isolation state, both CBs opened.
- State D: One CB reclosed, other remains open *("dead-line charging state").*
- State E: Final isolation state, the reclosed CB is re-tripped as there is a permanent fault.

States A, B and D are the most important states from the perspective of the developed fault location algorithm; states C and E contain no useful information relating to fault location. Consequently, the method only analyzes states A, B and D, which are re-denoted as pre-fault state, state 1 and state 2. During operation of the auto-reclose scheme, state 2 may differ, depending on which line-end CB is reclosed.

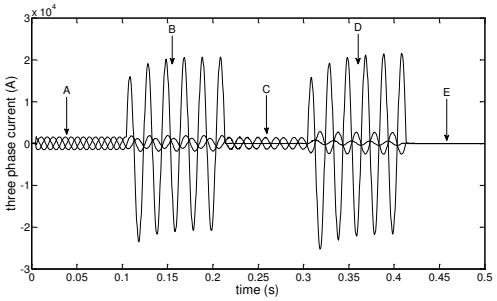

(a) Local CB tripped first in SPAR scheme

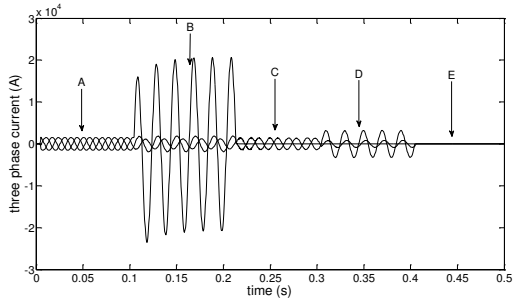

(b) Remote CB tripped first in SPAR scheme

Fig. 1. Currents during SPAR scheme operation: permanent fault

B. Modeling of electrical parameters during each state

The method relies on comparison of calculated states (based on the impedance model) with actual measurements taken during each state. This section describes how the various system states are modeled.

1) State 1 computation – during-fault state

According to superposition theory, the state 1 network can be represented as the sum of the pre-fault state network and the superimposed network, as shown in Fig.2. The superimposed network is defined as the network with all pre-fault system voltage sources shorted and three additional ideal voltage sources introduced in series with the fault impedance. The magnitude of the individual phase voltages of this three-phase source are equal to the pre-fault voltage at the fault position and the phase is shifted by 180° with respect to the pre-fault voltage. In the pre-fault network represented by Fig.2(a),

$$\mathbf{V_L} = \mathbf{AV_R} + \mathbf{BI_R} \quad (1)$$

$$\mathbf{I_L} = \mathbf{CV_R} + \mathbf{DI_R} \quad (2)$$

Where: $\mathbf{A} = \mathbf{D} = cosh\,\gamma d; \mathbf{B} = \mathbf{Z_c} \cdot sinh\,\gamma d;\ \mathbf{C} = \mathbf{Z_c^{-1}} sinh\,\gamma d.$

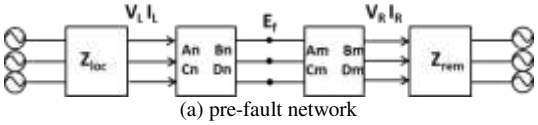

(a) pre-fault network

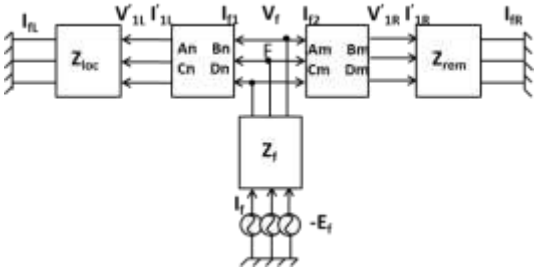

(b) superimposed network

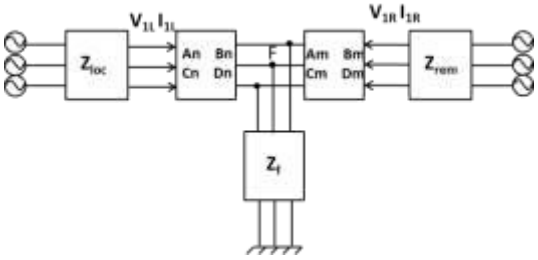

(c) during fault network

Fig.2. State 1 network calculation

A distributed line model is utilized to cater for the effects of parameter distribution. In Fig.2(a), the pre-fault network is separated into two sections around the fault location, which are:

(i) the local end to fault section $\begin{bmatrix}\mathbf{A_n} & \mathbf{B_n}\\ \mathbf{C_n} & \mathbf{D_n}\end{bmatrix}$

and

(ii) the fault to remote end section $\begin{bmatrix}\mathbf{A_m} & \mathbf{B_m}\\ \mathbf{C_m} & \mathbf{D_m}\end{bmatrix}$.

Where:

$\mathbf{A_n} = \mathbf{D_n} = cosh\,\gamma nd$

$\mathbf{B_n} = \mathbf{Z_c} \cdot sinh\,\gamma nd$

$\mathbf{C_n} = \mathbf{Z_c^{-1}} sinh\,\gamma nd$

$\mathbf{A_m} = \mathbf{D_m} = cosh\,\gamma(1-n)d$

$\mathbf{B_m} = \mathbf{Z_c} \cdot sinh\,\gamma(1-n)d$

$\mathbf{C_m} = \mathbf{Z_c^{-1}} sinh\,\gamma(1-n)d$

$\mathbf{V_L}$ and $\mathbf{I_L}$ are assumed to be known – in practice these values could be continually measured and stored in a "circular memory buffer" within a relay, with the prevailing values being stored for subsequent use upon detection of a fault and initiation of the fault location algorithm.

The general three phase fault model can be represented as:

$$\mathbf{Y_f} = \begin{bmatrix} \frac{1}{Rag+Rab+Rac} & -\frac{1}{Rab} & -\frac{1}{Rac} \\ -\frac{1}{Rab} & \frac{1}{Rbg+Rab+Rbc} & -\frac{1}{Rbc} \\ -\frac{1}{Rac} & -\frac{1}{Rbc} & \frac{1}{Rcg+Rac+Rbc} \end{bmatrix} \quad (3)$$

Note that R_{ij} is the fault resistance connected to the faulted phase, and i=j=a,b,c.g (denoting phases and ground).

If the fault involves only one value of resistance, then (3) can be simplified as shown below (other fault types are discussed in the section V):

$$\mathbf{Y_f} = \frac{1}{R_f}\mathbf{K} \quad (4)$$

Note that $\mathbf{K}$ is a fault matrix that denotes the fault type [18], using the followed method.

1. Compute,

$k_{i,j} = \begin{cases} -1, & \text{if } i \text{ and } j \text{ are involved in the fault} \\ 0, & \text{otherwise} \end{cases}$, i=j=a,b,c

2. Adjust the diagonal elements

$$k_{ii} = \sum_{j=a}^{j=c} |k_{ij}|, i = a,b,c$$

In this paper, single line to ground faults are investigated, therefore:

$$\mathbf{K} = \begin{bmatrix} 1 & 0 & 0 \\ 0 & 0 & 0 \\ 0 & 0 & 0 \end{bmatrix} \quad (5)$$

In the superimposed network shown in Fig.2(b), the local and remote end supply voltages are zero. Considering the distributed line model between the fault location and both local and remote ends, (6) and (7) can be obtained:

$$\begin{bmatrix}\mathbf{V_f}\\ \mathbf{I_{f1}}\end{bmatrix} = \begin{bmatrix}\mathbf{A_L} & \mathbf{B_L}\\ \mathbf{C_L} & \mathbf{D_L}\end{bmatrix}\begin{bmatrix}0\\ \mathbf{I_{fL}}\end{bmatrix} \quad (6)$$

$$\begin{bmatrix}\mathbf{V_f}\\ \mathbf{I_{f2}}\end{bmatrix} = \begin{bmatrix}\mathbf{A_R} & \mathbf{B_R}\\ \mathbf{C_R} & \mathbf{D_R}\end{bmatrix}\begin{bmatrix}0\\ \mathbf{I_{fR}}\end{bmatrix} \quad (7)$$

Where: $\mathbf{A_L} = \mathbf{A_n}; \mathbf{B_L} = \mathbf{A_n} + \mathbf{Z_{loc}B_n}; \mathbf{C_L} = \mathbf{C_n};$

$\mathbf{D_L} = \mathbf{C_n} + \mathbf{Z_{loc}D_n}; \mathbf{A_R} = \mathbf{A_m};$

$\mathbf{B_R} = \mathbf{A_m} + \mathbf{Z_{rem}B_m};$

$$\mathbf{C_R = C_m;\ D_R = C_m + Z_{rem} D_m}.$$

$\mathbf{Z_{loc}}$ and $\mathbf{Z_{rem}}$ depend on SCL1 and SCL2 and their respective X/R ratios.

Using (6) and (7), $\mathbf{I_{f1}}$ and $\mathbf{I_{f2}}$ may be represented in terms of $\mathbf{V_f}$ as follows:

$$\mathbf{I_{f1} = D_L B_L^{-1} V_f} \quad (8)$$

$$\mathbf{I_{f2} = D_R B_R^{-1} V_f} \quad (9)$$

In Fig.2(b), considering the path from the fault location to ground, the following can be derived:

$$\mathbf{I_f = (-E_f - V_f) Y_f} \quad (10)$$

$$\mathbf{I_f = I_{f1} + I_{f2}} \quad (11)$$

While $\mathbf{E_f}$ is the voltage at the fault point in pre-fault network

$$\mathbf{E_f = A_n V_L - B_n I_L} \quad (12)$$

Assuming n, R_f and $\mathbf{Z_{rem}}$ are known, $\mathbf{V_f}$ and $\mathbf{I_{f1}}$ can be solved through (8) to (11). Consequently, the local end voltage and current in the superimposed network are:

$$\begin{bmatrix} \mathbf{V'_{1L}} \\ \mathbf{I'_{1L}} \end{bmatrix} = \begin{bmatrix} \mathbf{A_n} & \mathbf{B_n} \\ \mathbf{C_n} & \mathbf{D_n} \end{bmatrix} \begin{bmatrix} \mathbf{V_f} \\ \mathbf{-I_{f1}} \end{bmatrix} \quad (13)$$

At the same time, the remote end voltage and current in the superimposed network are:

$$\begin{bmatrix} \mathbf{V'_{1R}} \\ \mathbf{I'_{1R}} \end{bmatrix} = \begin{bmatrix} \mathbf{A_m} & \mathbf{B_m} \\ \mathbf{C_m} & \mathbf{D_m} \end{bmatrix} \begin{bmatrix} \mathbf{V_f} \\ \mathbf{-I_{f2}} \end{bmatrix} \quad (14)$$

According to superposition theory:

$$\mathbf{V_{1L} = V_L + V'_{1L}} \quad (15)$$

$$\mathbf{I_{1L} = I_L + I'_{1L}} \quad (16)$$

$$\mathbf{V_{1R} = V_R + V'_{1R}} \quad (17)$$

$$\mathbf{I_{1R} = I_R + I'_{1R}} \quad (18)$$

2) State 2 computation – one CB reclosed

In state 2, there are two possible situations (for both SPAR and TPAR), depending on whether the local or remote CB is reclosed initially. In summary, there are four possible scenarios relating to state 2:

A. SPAR - local end CB reclosed initially;
B. SPAR - remote end CB reclosed initially;
C. TPAR - local end CB reclosed initially;
D. TPAR - remote end CB reclosed initially.

The computations for each scenario are described in the following sections.

a) Situation A: SPAR - local end CB reclosed initially

As in the previous section, superposition theory has been applied in this situation. The state 2 network (Fig 3b) is the sum of state 1(Fig.2c) and state 2 superimposed networks (Fig 3a). In the state 2 superimposed network, the tripped pole of the CB is represented as a current source which is equal to the fault current supplied by the remote end in state 1 (but anti-phase):

$$\mathbf{I'_{2Ra} = -I_{1Ra}} \quad (19)$$

In Fig 3(a), the distributed network section from the fault point to the local end is represented as in equation (6).

The path from the fault point to ground is expressed as:

$$\mathbf{I_f = Z_f^{-1} V_f = Y_f V_f} \quad (20)$$

From (19) and (20), we can obtain:

$$\mathbf{I_{f2} = I_{f1} + I_f = \left(Y_f + D_L B_L^{-1}\right) V_f} \quad (21)$$

Where: $\mathbf{I_{f1}}$ is the current flow through $\mathbf{Z_f}$, which has been expressed in equation (8).

The network section from the remote end to the fault point is represented as:

$$\mathbf{V'_{2R} = A_m V_f + B_m I_{f2}} \quad (22)$$

$$\mathbf{I'_{2R} = C_m V_f + D_m I_{f2}} \quad (23)$$

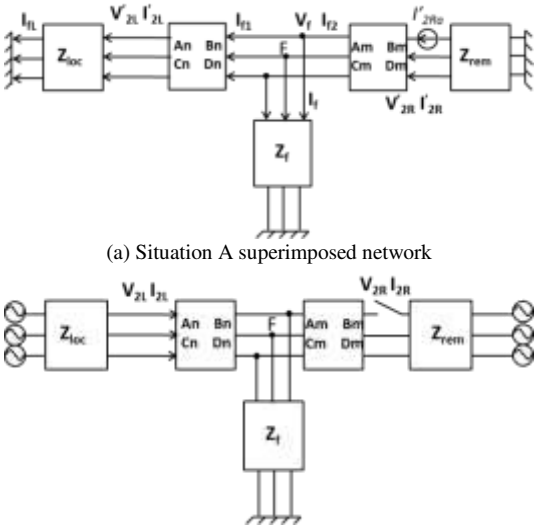

(a) Situation A superimposed network

(b) Situation A state 2 of network

Fig 3 State 2 network calculation

Eliminating $\mathbf{V_f}$ from (22) and (23) using (21) gives:

$$\mathbf{V'_{2R} = X\, I_{f2}} \quad (24)$$

$$\mathbf{I'_{2R} = Y\, I_{f2}} \quad (25)$$

Where, $\mathbf{I_{f2}}$ is a 3×1 matrix and $\mathbf{X}$, $\mathbf{Y}$ are 3×3 matrices, represented as:

$$\mathbf{X} = [R_f^{-1}\mathbf{K} + \mathbf{D_L B_L^{-1}}]^{-1}\mathbf{A_m} + \mathbf{B_m} \quad (26)$$

$$\mathbf{Y} = [R_f^{-1}\mathbf{K} + \mathbf{D_L B_L^{-1}}]^{-1}\mathbf{C_m} + \mathbf{D_m} \quad (27)$$

$\mathbf{X}$ and $\mathbf{Y}$ depend on n, R_f and $\mathbf{Z_{rem}}$. Assuming n, R_f and $\mathbf{Z_{rem}}$ are known, $\mathbf{V_f}$ can be solved using equations (21) to (27).

In the superimposed network, the network section from the fault point to the local end can be represented as:

$$\begin{bmatrix} \mathbf{V_f} \\ \mathbf{I_{f1}} \end{bmatrix} = \begin{bmatrix} \mathbf{A_L} & \mathbf{B_L} \\ \mathbf{C_L} & \mathbf{D_L} \end{bmatrix} \begin{bmatrix} \mathbf{0} \\ \mathbf{I'_{2L}} \end{bmatrix} \quad (28)$$

It is assumed that $\mathbf{I'_{2L} = I_{fL}}$. Equation (28) can be solved for $\mathbf{I'_{2L}}$, and consequently, $\mathbf{V'_{2L} = Z_{loc} I'_{2L}}$.

According to superposition theory, the local voltage $\mathbf{V_{2L}}$ and current $\mathbf{I_{2L}}$ in state 2 are:

$$\mathbf{V_{2L} = V_{1L} + V'_{2L}} \quad (29)$$

$$\mathbf{I_{2L} = I_{1L} + I'_{2L}} \quad (30)$$

Accordingly, the local voltage and current during both states 1 and 2 can be estimated using values for n, R_f and SCL2. This is the basis of the method; when the local voltages and currents match the model-estimated values, then the corresponding fault location, fault resistance and remote SCL can be estimated with high accuracy (as shown in Fig. 4).

b) Situations B, C and D

The computation used in situations B, C and D are similar to situation A. Open CBs are represented as current sources and the superposition method is applied to derive the voltage and current phasors.

III. THE FAULT LOCATION ALGORITHM

A. Overview

There are three main elements to the algorithm: fault data processing; initial range estimation; and fault location estimation. The fault data element extracts the fundamental frequency phasor from the actual sampled fault data. The initial range estimation element provides initial ranges of possible n, R_f and SCL2 using measured data to "focus" on an initial range of possible fault locations and to optimize the search space. The fault location element is based on transmission line modeling as described in section II, which estimates local voltage and current for various combination groups of n, R_f and SCL2until a match is found. The location element itself comprises three main stages of operation:

- transmission line modeling;
- comparison;
- storing of interim output for use in next state.

The transmission line modeling is based on the auto reclosing calculation, which calculates the anticipated currents and voltages during different SPAR/TPAR states for a range of potential fault locations. It is used to iteratively generate the voltage and current data associated with the range of potential n, R_f and SCL2.In state 1, the associated ranges are estimated using measured data. The comparison stage matches the voltage and current data generated by the transmission line model with the actual measured data. If the matching process is successful, the algorithm records the corresponding values of n, R_f and SCL2 (recording stage). The modeling, comparison and storing stages are repeated until the solution is found and the comparison condition is satisfied as shown in Fig. 4. After state 1iteration, new ranges for each of the three parameters are formed and the process proceeds to state 2. As progress through each of the states is made, the possible ranges of locations reduce and the final accurate fault location is obtained. At the final state, an averaging process is used to produce the final estimations of fault location in the most accurate fashion.

B. Pre-estimation of candidate ranges

The main principle of the proposed fault location method is to compare the measured data with the results of voltage and current phasor model-based computations, and to obtain the most likely combination group of R_f, n and SCL2. Before state 1, the analysis of measured data is used to initially limit the ranges of each variable using a conventional impedance-based fault location method.

n pre-estimation range is calculated using the Takagi fault location[2] as shown in equation (31).

$$fl = \frac{Im(V_{1L} I^*_{sup})}{Im(I_{1L} Z_l I^*_{sup})} \tag{31}$$

Where, I^*_{sup} is the conjugate of the superimposed current, which is equal to$I_{sup} = I_{1L} - I_L$.

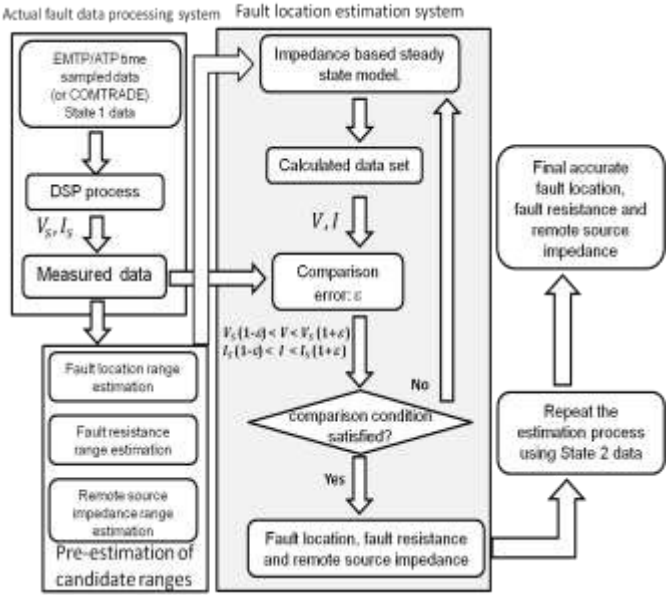

Fig.4 Fault location algorithm

The Takagi method improves fault location accuracy by reducing the effects of R_f and load flow on location accuracy. The key to the success of the method is that, theoretically, I_{sup} has the same angle as the fault current flowing through R_f. However, as R_f, increases, the angular difference between fault current and I_{sup} increases, which leads to an increased fault location estimation error. Fig 5 shows the accuracy of the Takagi method for various scenarios. It is found that the majority of the accuracy errors are less than 15% until R_f reaches 100Ω. Consequently, the initial fault location pre-estimation range is set to $[fl - 15\%, fl + 15\%]$. Note that in cases where $fl - 15\% < 0\%$, the range is set to $[0\%, fl + 15\%]$, while in the case of $fl + 15\% > 100\%$, the range is set to $[fl - 15\%, 100\%]$.

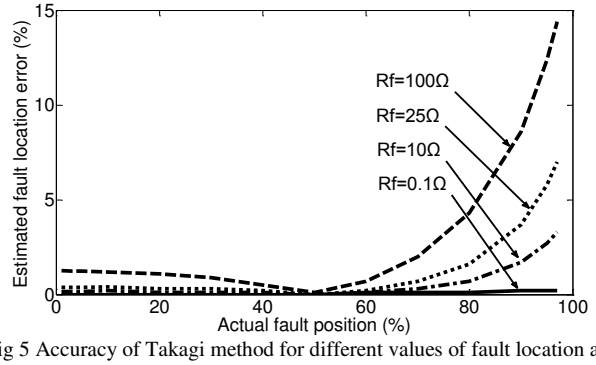

Fig 5 Accuracy of Takagi method for different values of fault location and resistance (remote end infeed 15GVA)

The range of SCL2 in this study is 5-30GVA, which is representative of most transmission system fault levels, but could be extended if required. The voltage and current are obtained from measured data at this stage, the initial n range is estimated using Takagi method and the range for SCL2 is assumed (5-30GVA in this case). To establish the initial range for R_f, the assumed minimum and maximum values for n and SCL2 are used in conjunction with equations describing state 1 (3)-(19) and measured values of voltage and current. For all four possible combinations of n and SCL2 (i.e. n_min, SCL2_min; n_min, SCL2_max; n_max, SCL2_min; n_max, SCL2_max) four different R_f values are calculated and the minimum and maximum values of the four are used to form the boundaries of the initial R_f range.

C. Comparison error and averaging technique

Both voltage and current are used for comparison between measured data and algorithm-calculated data. Considering current, the phasor magnitudes and angles are analyzed in the comparison; a similar technique is used for voltage:

$$I_{m\_mag}(1-\varepsilon) < I_{c\_mag} < I_{m\_mag}(1+\varepsilon) \quad (32)$$

$$I_{m\_ang}(1-\varepsilon) < I_{c\_ang} < I_{m\_ang}(1+\varepsilon) \quad (33)$$

Note that I_{m_mag} and I_{m_ang} are the magnitude and angle of measured current while I_{c_mag} and I_{c_ang} are the magnitude and angle of calculated current. ε is the comparison tolerance.

If the result of the fault location estimation system matches the measured data, the values of n, SCL2 and R_f are recorded as potential solutions.

The tolerance used in the comparisons determines the number of candidate solutions (each solution comprising a value for R_f, SCL2 and n). Greater tolerances will result in a greater number of candidate solutions. The tolerance is iteratively increased from an initial setting value until the number of candidate solutions at each state is greater than a certain value. In the following case study, the initial comparison tolerance is set to 0.1% and the minimum number of candidate solutions for state 1 and state 2 are 100 and 10 respectively.

There are cases were there may be more than one candidate at the final stage. It has been established, through exhaustive testing, that these are typically closely grouped around similar values of location, SCL and fault resistance. Thus, in such cases, the final output estimations can be derived by averaging the values for n, SCL2 and R_f.

IV. CASE STUDY

In this section, ATP simulated data is used to represent measurement data in order to evaluate the performance algorithm. A modified Least Squared Method [16] has been designed to improve the accuracy of fundamental frequency phasor extraction by reducing the negative effects of decaying DC offset and other unexpected noise.

In the model shown in Fig 6, the local SCL is set to 15GVA and the X/R ratio of both local and remote ends is 30**.** The positive and zero sequence line impedance values are

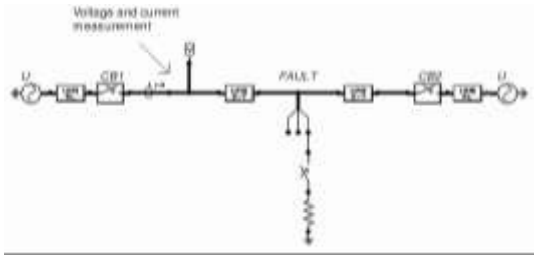

Fig 6 ATP transmission line model

Z_{L1}=0.02+j0.25Ω/km and Z_{L0}=0.10+j0.76Ω/km, while positive and zero sequence shunt capacitive reactance values are Y_{L1}=0+j4.7e^{-6}Ω/km and Y_{L0}=0+j2.5e^{-6}Ω/km. The transmission line is represented by the distributed parameter three-phase transposed model in ATP. A constant fault resistance model is used. The increments of n and SCL2 are set to 0.1% and 1GVA respectively. The increment of R_f depends on the initial range estimate using the Takagi method as described earlier. In the case where the maximum initial range estimate of R_f is less than 5Ω, the increment is set to 0.01Ω; otherwise, the increment is set as 0.1Ω. The local short circuit level (SCL1) is set to 15GVA in the simulations. The impact of assumed values of SCL1 and SCL2 (for 5GVA, 15GV and 30GVA) on location accuracy has been investigated, and the maximum introduced error is less than 0.5%, so the values of SCL 1 and SCL2 used has been set to 15GVA for all results presented in this paper.

A. Example of operation

In this example, the fault is assumed to occur at 50km (50% of line length from measurement point), the fault resistance R_f is set as 10Ω, the SCL2 is set as15GVA and the prefault power flow in the line is 1.5GVA. In this example, the increments of n, Rf and SCL2 are 0.1km, 0.1Ω and 1GVA respectively. The estimated fault location using the TAKAGI method is 51.1%.

Table I shows the progression and divergence of the estimated values during the state-by-state estimation process.

TABLE I
INTERIM AND FINAL OUTPUTS FROM FAULT LOCATION ESTIMATION SYSTEM

	Range n (km)	Range R_f (Ω)	Range SCL2 (GVA)	Candidates
Pre-estimation	35.1-65.1	6-16	5-30	750000
State 1	48.0-51.8	8.8-11	15	283
State 2	49.6-50.3	10	15	14
Final result	49.95	10	15	1

It is clear that each progression produces a drastic reduction in the number of candidates. In this example, the final output value is computed by averaging the 14 candidates from state 2.

B. Comparison with Takagi method

Table II shows the performance of the Takagi method versus the method reported here for different values of SCL2, R_f and all possible fault locations, from 1% to 100% along the line. The estimated fault location error is determined by (34). In the comparison, a scenario using a SPAR scheme is used to assess performance.

$$Error = \frac{(estimated\ fault\ location - actual\ fault\ location)}{line\ length} \quad (34)$$

The Takagi method reduces the effect of fault resistance by reducing the angle difference between the current flowing through the fault resistance and the superimposed current. However, the angle difference still increases proportionately with n, R_f and uncertainty relating to the value of SCL2. The method reported in this paper addresses these deficiencies and significantly reduces such negative effects. This indicates that the proposed fault location method addresses certain scenarios where the Takagi method can be influenced by the uncertainty of R_f and SCL2 and may not be highly accurate, such as where faults are located very close to the remote end (i.e. greater than 90% of the line length) and faults with high resistance.

TABLE II
COMPARISON WITH TAKAGI METHOD

n (%)	R_f (Ω)	SCL2 (GVA)	Maximum error (%)		Mean error (%)	
			Takagi	Proposed	Takagi	Proposed
1-100	0.01	5	0.78	0.20	0.22	0.08
1-100	25	5	5.50	0.21	1.83	0.09
1-100	100	5	9.71	0.50	4.10	0.19
1-100	0.01	15	0.82	0.30	0.25	0.10
1-100	25	15	6.10	0.20	1.85	0.12
1-100	100	15	14.7	0.40	6.30	0.15
1-100	0.01	30	0.95	0.30	0.30	0.12
1-100	25	30	9.80	0.21	2.07	0.09
1-100	100	30	15.6	0.50	7.33	0.15

C. Algorithm evaluations

The performance of the location method is presented for all possible auto-reclose scheme scenarios (i.e. SPAR LOCAL, SPAR REMOTE, TPAR LOCAL, and TPAR REMOTE - (note that, for example, SPAR LOCAL denotes a SPAR scheme where the local end CB recloses first), for all possible fault positions and fault resistances (from 0-100Ω).

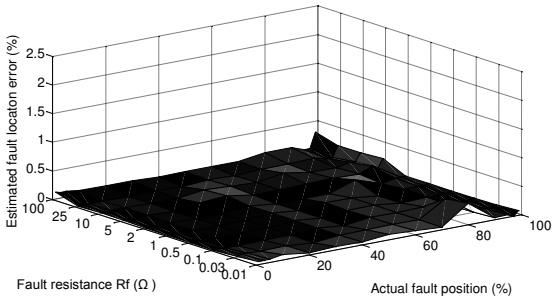

(a) SPAR LOCAL

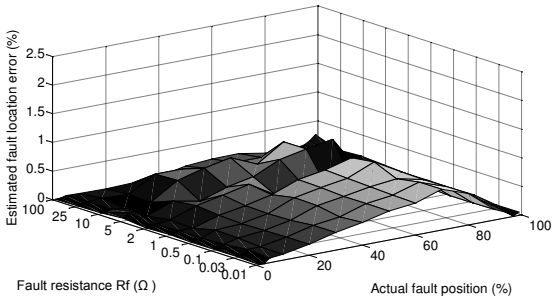

(b) SPAR REMOTE

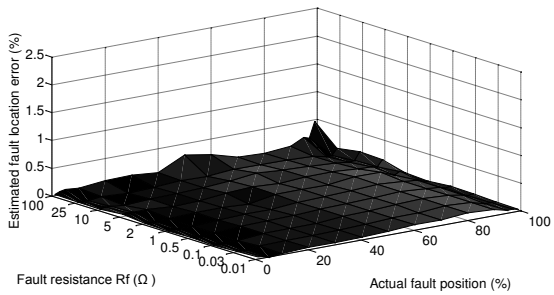

(c) TPAR LOCAL

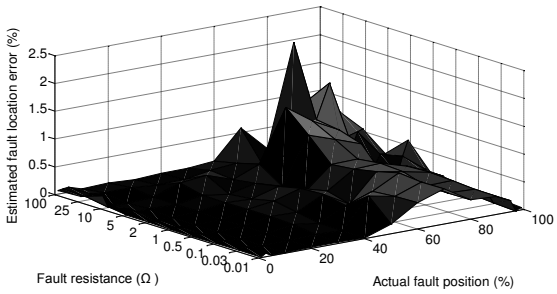

(d) TPAR REMOTE

Fig 7 Accuracy of proposed method for all situations

Fig 7 illustrates the performance. It is clear that the proposed method can achieve very high accuracy in the majority of situations, with average error of well under 1% (and often under 0.1%) in all cases. It is only in scenarios where R_f and n are high (representative of high resistance faults close to the remote end of the line) that relatively larger errors (up to 2%) are encountered. However, errors are consistently lower than those associated with the Takagi method.

V. DISCUSSION AND FUTURE WORK

In this paper, only single line to ground faults have been analyzed. The fault matrix **K** represents different fault types through varying the elements. The reported method is capable of locating fault types which involve one fault resistance (i.e. single line to ground fault, line to line fault). For faults involving more than one resistance (e.g. line-line-ground faults), the value of the fault resistance R_f and the grounding resistance R_g may be different. In such cases, the fault matrix **K** cannot be directly used. However, the grounding fault resistance R_g can be added to the fault matrix $\mathbf{Y_f}$ (refer to equation (3)) as an unknown variable in the iteration. In the future, other fault types should be investigated**.** As the method is iterative, the possibility of non-convergence may of course be a risk. However, during all case studies with a wide range of realistic transmission line and fault parameters numerical convergence has never been encountered.

Phenomena such as arcing voltage and CT saturation can degrade measured data and negatively influence the accuracy of any impedance based fault location techniques. Investigation of the impact of these phenomena on the reported techniques should be carried out as future work. Furthermore, different system configurations and the impact of dynamically changing fault resistance as well as variation (or errors) in primary system parameters (e.g. transmission line parameters, mutual

impedance calculation and variation) should be investigated and testing of the system on actual recorded data will be undertaken.

In terms of implementation of the system, standard numerical protection hardware, possibly with extension to include more memory and perhaps with an additional processor dedicated to fault location, could be used. Future work with the industrial partners will be concerned with addressing the implementation of the method.

VI. Conclusions

A new fault location algorithm, which is based on analysis of measurements during the various states of SPAR and TPAR scheme operation, has been presented. The system employs a model-based approach, comparing simulation-produced candidate solutions (comprising values of n, R_f and SCL2)with actual measurements at each stage of analysis, to progressively focus in on a final solution. The algorithm operates solely on single ended data. The method is less affected by variations in fault resistance than for other methods (notably the established Takagi method) and has been shown to be capable of providing estimates for fault resistance and remote short circuit levels. It should be relatively economical and easy to implement; only local end data is needed. Furthermore, as fault location is most useful for location of permanent faults (where repair crews need accurate location information to effect timely repairs) the operation of the system, while not instantaneous, should provide the output information within tens of seconds, which is sufficient in the context of this application.

Acknowledgment

The authors wish to gratefully acknowledge the financial and technical support of Toshiba International (Europe) Limited.

References

[1] Saha,M.M.; Izykowski,J.; Rosolowski, E.;, “Fault Location on Power Network”, in Vasteras Sweden, Springer London Dordrecht Heidelberg, New York, pp.1-4, 17-26, 2010

[2] Takagi, T.; Yamakoshi, Y.; Yamaura, M.; Kondow, R.; Matsushima, T.;, "Development of a New Type Fault Locator Using the One-Terminal Voltage and Current Data", Power Apparatus and Systems, IEEE Transactions on, vol.PAS-101, no.8, pp.2892-2898, Aug.1982

[3] Zimmerman, K.; Costello, D.;, "Impedance-Based Fault Location Experience", Rural Electric Power Conference, 2006

[4] Edmund, A; Schweitzer III, O, "Evaluation and development of Transmission Line Fault-Locating Techniques which uses Sinusoidal Steady-State Information" , presented at the Ninth Annual Protective Relay Conference, Spokane, Washington, Oct. 1982.

[5] Eriksson, L, et al., "An Accurate Fault Locator With Compensation For Apparent Reactance In The Fault Resistance Resulting From Remore-End Infeed," Power Apparatus and Systems, IEEE Transactions on, vol. PAS-104, pp. 423-436, 1985.

[6] Kawady, T.; Stenzel, J.; Sachdev et al, "Investigation of practical problems for digital fault location algorithms based on EMTP simulation", Transmission and Distribution Conference and Exhibition 2002: Asia Pacific. IEEE/PES, vol.1, no., pp.118-123, 6-10 Oct.2002

[7] Izykowski, J.; Rosolowski, E.; Balcerek, P.; Fulczyk, M.; Saha, M.M.;, "Accurate Noniterative Fault Location Algorithm Utilizing Two-End Unsynchronized Measurements", Power Delivery, IEEE Transactions on, vol.25, no.1, pp.72-80, Jan.2010

[8] Brahma, S.M.; Girgis, A.A.;, "Fault location on a transmission line using synchronized Voltage measurements", Power Delivery, IEEE Transactions on, vol.19, no.4, pp.1619- 1622, Oct.2004

[9] Bo, Z.Q.; Weller, G.; Jiang, F.; Yang, Q.X.;, "Application of GPS based fault location scheme for distribution system", Power System Technology, 1998. Proceedings. POWERCON '98. 1998 International Conference on, vol.1, no., pp.53-57, 18-21 Aug.1998

[10] Chen, Z.; Luo C.; Su, J.; Wu, X.;, "A fault location algorithm for transmission line based on distributed parameter", Developments in Power System Protection, 2001, Seventh International Conference on (IEE), vol., no., pp.411-413, 2001

[11] Aurangzeb, M.; Crossley, P.A.; Gale, P.;, "Fault location using the high frequency travelling waves measured at a single location on a transmission line", Developments in Power System Protection, 2001, Seventh International Conference on (IEE) , vol., no., pp.403-406, 2001

[12] Gale, P.F.; Taylor, P.V.; Naidoo, P.; Hitchin, C.; Clowes, D.;, "Travelling wave fault locator experience on Eskom's transmission network", Developments in Power System Protection, 2001, Seventh International Conference on (IEE), vol., no., pp.327-330, 2001

[13] Edwards, A.; van Heerden, R.; Chowdhury, S.; Chowdury, S.P.; Kang, H.;, "Fast auto-reclose function for 765 kV lines in the proximity of resonant line voltages",Developments in Power System Protection (DPSP 2010). Managing the Change, 10th IET International Conference on, vol., no., pp.1-4, 29 Mar. 2010-1 Apr. 2010 doi: 10.1049/cp.2010.0257

[14] Brewis, K.;, "Integrated protection and auto-reclose control of source circuit breakers",Improving Supply Security on 11kV Overhead Networks, IEE Colloquium on, vol., no., pp.9/1-9/4, 1988

[15] GUO Fang-xi; HAO Yong-jin; XIAO Yin;, “Time integrating improvement of Single Phase Reclose Scheme using Fiber-optic current differential protection”, Shanxi Electric Power, No.5(Ser. 141), pp.15-17, Oct.2007

[16] Rosolowski E; Izykowski J; Kasztenny B;, “Adaptive measuring algorithm suppressing a decaying DC component for digital protective relays”, Eletr Power Syst Res. 60(2):99-105, 2001

[17] Ji, L.; Booth, C.; Dysko, A.; Kawano, F.; Baber, G.;, “Improving fault location by analysis of electric parameters during circuit breaker operation”, Paper 48, presented at 17th Power System Computation Conference (2011), Stockholm, Sweden

[18] M. M. Saha, et al., "A new accurate fault locating algorithm for series compensated lines," in Power Engineering Society 1999 Winter Meeting, IEEE, 1999, p. 956 vol.2

Liang Ji received his B.Eng. and Ph.D. degrees in Electronic and Electrical Engineering from the University of Strathclyde, UK. He is presently a lecturer in the college of Electrical Engineering in Shanghai University of Electrical Power, Shanghai.

Campbell Booth received the B.Eng. and Ph.D. degrees in Electronic and Electrical and engineering from the University of Strathclyde, Glasgow, UK. He is currently a Senior Lecturer with the Institute for Energy and Environment, Department of Electronic and Electrical Engineering, University of Strathclyde.

Adam Dyśko (M’06) received the M.Sc. degree from the Technical University of Łódź, Poland, in 1990, and the Ph.D. degree from the University of Strathclyde, Glasgow, U.K., in 1998. Currently, he is a Lecturer in the Department of Electronic and Electrical Engineering, University of Strathclyde.

Fumio Kawano received his B.S. degree from Tokyo Institute of Technology and M.S. degree in Engineering from The University of Tokyo, Japan, in 1998 and 2000 respectively. He joined Toshiba International (Europe) Limited in October 2008, and is currently working in the UK. He is a member of IEC TC95 MT4,IEEJ, IET and IEEE.

Phil Beaumont (SM’99) read Electrical Engineering at Leeds in the UK and graduated with a BSc (Hons) degree. Phil is active in a number of Cigré and IEEE PSRC WGs and is IEC TC95 MT4 Secretary. He is a Chief Specialist with Toshiba International (Europe)Limited, a Senior Member of the IEEE and a Fellow of the IET.